Title	Size-dependent Exciton Recombination Dynamics in Single CdS Nanowires beyond the Quantum Confinement Regime
Author(s)	Liu, Xinfeng; Zhang, Qing; Xing, Guichuan; Xiong, Qihua; Sum, Tze Chien
Citation	Liu, X., Zhang, Q., Xing, G., Xiong, Q., & Sum, T. C.(2013). Size-dependent Exciton Recombination Dynamics in Single CdS Nanowires beyond the Quantum Confinement Regime. The Journal of Physical Chemistry C, 117 (20), 10716–10722.
Date	2013
URL	http://hdl.handle.net/null
Rights	© 2013 American Chemical Society.

Size-dependent Exciton Recombination Dynamics in Single CdS Nanowires beyond the Quantum Confinement Regime

Xinfeng Liu, [†] *Qing Zhang,* [†] *Guichuan Xing,* [†,‡] *Qihua Xiong* [†,⊥] *and Tze Chien Sum*[†,‡,#*]

[†]Division of Physics and Applied Physics, School of Physical and Mathematical Sciences, Nanyang Technological University, 21 Nanyang Link, Singapore 637371

[⊥]Division of Microelectronics, School of Electrical and Electronic Engineering, Nanyang Technological University, Singapore 639798

[‡]Energy Research Institute @ NTU (ERI@N), Nanyang Technological University, 50 Nanyang Drive, Singapore 637553

[#]Singapore-Berkeley Research Initiative for Sustainable Energy, 1 Create Way, 138602, Singapore

*To whom correspondence should be addressed, Email address: tzechien@ntu.edu.sg

ABSTRACT

A deep understanding of the size, surface trapping and scattering effects on the recombination dynamics of CdS nanowires (NWs) is a key step for the design of on-demand CdS-based nanodevices. However, it is often very difficult to differentiate these intertwined effects in the NW system. In this article, we present a comprehensive study on the size-dependent exciton recombination dynamics of high quality CdS NWs (with diameters from 80 to 315 nm) using temperature dependent and time-resolved photoluminescence (TRPL) spectroscopy in a bid to distinguish the contributions of size and surface effects. TRPL measurements revealed two distinct processes that dominate the band edge recombination dynamics – a fast decay process (τ_1) originating from the near-surface recombination and a slower decay process (τ_2) arising from the intrinsic free exciton A (FXA) decay. With increasing NW diameters, τ_1 increases from ~0.10 ns to ~0.42 ns due to the decreasing surface-to-volume ratio of the NWs; while τ_2 increases from ~0.36 ns to ~1.21 ns due to decreased surface scattering in the thicker NWs – as validated by the surface passivation and TRPL studies. Our findings have discerned the interplay between size and surface effects and advanced the understanding of size-dependent optoelectronic properties of one-dimensional semiconductor nanostructures for applications in surface- and size-related nanoscale devices.

Keywords: Semiconductor nanowires; Lifetime; Surface passivation; Surface trapping; Surface scattering;

INTRODUCTION

Remarkable progress in material science has made it possible to fabricate high quality semiconductor nanostructures with large surface-to-volume ratio and with dimensions that are comparable to the characteristic length scales of excitons and free carriers.[1-4] Size and surface effects (*e.g.*, surface trapping and scattering) still exert a considerable influence on their optoelectronic properties – resulting in properties that are distinct from the bulk.[5-8] However, such effects are often highly entangled – for example decreasing the size of the nanowire (NW) diameter will induce a larger surface-to-volume ratio – making it extremely difficult to distinguish their respective contributions.

One-dimensional (1-D) semiconductor nanostructures such as NWs have been under scrutiny for applications as optically and electrically driven lasers, photodetectors and waveguides *etc*.[9] CdS NWs hold great potential for nanoscale optoelectronic applications.[6, 7, 10-12] Due to its large exciton binding energy of ~28 meV (which is slightly larger than the thermal energy k_BT ~25 meV at room temperature), highly efficient excitonic processes are expected and these have been shown to dominate the optical properties of CdS at room temperature (RT).[13, 14] Recently, plasmon lasers have been successfully demonstrated using the Ag film/MgF_2/CdS NWs hybrid system.[15, 16, 17] Modulation of the excitonic radiative decay rates in CdS NWs have also been demonstrated through careful geometrical design of CdS-SiO_2-Ag whispering-gallery plasmonic NWs.[18] Most recently, phonon-assisted anti-Stokes photoluminescence in CdS nanobelts have also been demonstrated (leveraging on their strong exciton-phonon coupling properties). This led to the first realization of solid-state

semiconductor-based laser cooling.[19] The efficiency of the laser cooling process is strongly dependent on the exciton recombination properties, *i.e.*, non-radiative exciton decay processes involved in surface trapping, resulting in a heating effect. Thus, a good understanding of the carrier dynamics in light of the various competing radiative and non-radiative pathways is essential for tailoring the optoelectronic properties of CdS NW-based photonic devices.

Previously, the impact of surface trap states on the exciton dynamics have been extensively studied in semiconductor quantum dots and NWs.[20-23] For example, Kambhampati *et. al.* unraveled the physical structure of quantum dots and obtained a clear understanding of the resultant electronic structure and dynamics with colloidal CdSe quantum dots as a test bed.[20] Block *et. al.* demonstrated the feasibility of using multi-resonant methods to probe the quantum state dynamics of interface states in nanostructures.[21] Vietmeyer *et. al.* studied the carrier recombination dynamics in individual CdSe NWs with diameters ~20 nm.[22] Lo *et. al.* conducted systematic studies on the charge carrier trapping and acoustic phonon modes in single CdTe NWs of diameter ~30 nm by transient absorption microscopy.[23] However, in these cases, the diameters of the quantum dots are comparable to the Bohr radius of the bulk semiconductors; and the diameters of the NW samples are ~20-30 nm – at a size where surface effects have a dominating influence. Detailed knowledge on the interplay between the size and surface effects on the exciton recombination dynamics in CdS NWs with diameters beyond the quantum confinement regime (*e.g.*, from 80 to 315 nm), is

presently still lacking. Elucidating the relationship between the size and surface effects on the exciton recombination dynamics in CdS NWs is the main focus of this work.

Surface passivation has often been used to improve the optical quality of NWs and modulate the effects of traps formed by dangling bonds and adsorbed species on NW surfaces. For example, Vugt *et. al.* passivated CdS NWs using atomic layer deposition (ALD) treatment and improved their optical quality.[24] Through photo-assisted surface passivation, they also reported an increase of the PL intensity in InP NWs.[25] Park *et. al.* demonstrated that the device characteristics of NW field-effect transistors (FETs) improved significantly after polyimide coating of the nanorod surface;[26] and Chang *et. al.* also reported improved NW FET device performance following SiO_2/Si_3N_4 passivation.[27]

In this work, a comprehensive temperature dependent PL and TRPL study on the size-dependent exciton decay dynamics in high quality CdS NWs fabricated by the vapor-liquid-solid (VLS) method is performed. The two band edge (BE) exciton decay channels are respectively identified as the surface states related non-radiative recombination (*i.e.*, with a short lifetime τ_1) and the free-exciton A (FXA) radiative recombination (*i.e.*, with a longer lifetime τ_2,). As the NW diameter decreases from 315 nm to 80 nm, the FXA decay rate increases monotonically. Through surface passivation treatments, TRPL measurements validate that the increasing FXA decay rate with decreasing dimensions stems from the enhanced surface scattering in the thinner NWs. In tandem, the surface states related non-radiative decay rate also increases with decreasing NW diameter as a result of the larger surface-to-volume ratio in the thinner NWs. These findings shed new light on the interplay of

the size and surface effects on the exciton recombination dynamics in CdS NWs and advance our understanding on the size-dependent optoelectronic properties of related 1-D semiconductor nanostructures.

EXPERIMENTAL METHODS

The CdS NWs were synthesized using the vapor-liquid-solid technique described previously.[6, 14] X-ray diffraction data were obtained using a Japan Rigaku D/MAX-240 type diffractometer equipped with graphite-monochromatized Cu K_α radiation (α = 1.54178 Å). For single NW measurements, the sample was first dispersed from the grown substrate into an ethanol solution and then subsequently deposited onto a silicon substrate (with a 300 nm thick SiO_2 layer). Both scanning electron microscopy (JEOL7001F FE-SEM) and high-resolution transmission electron microscopy (HRTEM, Tecnai G2) were used to assess the morphology and the crystalline quality of the individual CdS NWs. Spatially-resolved photoluminescence (PL) measurements of the individual CdS NWs were performed using a confocal microscope with a long working distance 50× objective (Nikon Objective, NA = 0.55) and a continuous wave (CW) laser (405 nm wavelength) as the excitation source. The PL emission was spectrally resolved with a monochromator (PI Acton, Spectra Pro 2500i) and collected with a TE-cooled charge CCD (PI, PIXIS-400B). Temperature-dependent PL (77 to 300 K) was performed using a liquid-nitrogen-cooled cryostat (Janis ST-500, Microscope Cryostat). For TRPL measurements, frequency doubled pulses (400 nm) from a Titanium: Sapphire oscillator (120 fs, 76 MHz at 800 nm) were used as the excitation source. The TRPL spectra were obtained using a streak camera system (Optronics GmbH) with an

ultimate temporal resolution of 6 ps (at a scan speed of 100 ps/mm) when operated in the synchroscan mode. Surface modification/passivation of the CdS NW surface was achieved by spin coating a thin layer of PMMA (~200 nm) over the NWs.

RESULTS AND DISCUSSIONS

Figure 1(a) shows the XRD pattern of the as-grown CdS NWs, where they were found to exhibit a hexagonal wurtzite (hexagonal) phase. Figure 1(b) shows a typical PL spectrum from a single CdS NW measured at room temperature, where the sample gives a very strong BE emission (~2.42 eV), but no obvious surface related emission from the lower energy region around 1.8 eV – thus attesting the high crystal quality of the samples.[28, 29] Representative TEM images of a NW are shown in Figure 1(b) inset, which reveals that the NW is relatively uniform. The HRTEM image shows that the CdS NWs are single crystalline, with a measured lattice spacing of ~0.33 nm – corresponding to the [002] lattice plane of hexagonal CdS.

Figure 1(c) shows the low temperature (77 K) PL spectrum of the sample where only the dominating BE emission (~2.50 eV) in the range of 2.30–2.58 eV is plotted for clarity. The experimental data (open circles) can be well-fitted with a least-squares fit of multiple Gaussian functions (solid red line). The respective deconvolved Gaussian peaks are plotted in solid blue lines and their peak positions/assignments are tabulated in Figure 1(c) inset. Our assignment is based on the following analysis: the CdS valence band is split into three non-degenerate energy levels under the crystal field and spin-orbit interactions – giving rise to FXA, FXB and FXC excitonic levels.[30] The emission peak at 2.532 eV, which is close to

the energy level of the free exction A in wurtzite CdS, is thus assigned as the FXA emission. Next, the peak at ~2.552 eV can be assigned to the free exction B (FXB) since the energy difference between itself and FXA is ~20 meV, which is close to the reported values (~19 meV).[11, 16] Given that the longitudinal optical (LO) phonon energy of CdS is around 40 meV,[11, 31, 32] the next three peaks (2.511, 2.471 and 2.432 eV) on the lower energy side of the NBE can be assigned to FXB-LO and FXB-2LO and FXB-3LO, respectively. The distinct appearance of the FXA, FXB and the third order phonon replica attests the high quality nature of these CdS NW samples.

Figure 2(a) shows the normalized temperature-dependent PL spectra of a CdS NW with a diameter of ~200 nm taken from 77 to 300 K. At low temperatures (<120 K), the FXB emission peaks can be resolved, which is consistent with the report by Thomas *et al.*[33] As the temperature increases further to >180 K, thermal broadening resulted in only a single broad BE emission peak being observed. The center of the FXA peak redshifts with increasing temperatures. The temperature dependence of the FXA and FXB peak energies as well as those of FXB-LO and FXB-2LO are shown in Figure 2(b). This temperature dependence of the CdS NW exciton energy can be described by the well-known Varshni's law:

$$E(T) = E(0) - \frac{\alpha T^2}{T + \beta}, \qquad (1)$$

where $E(0)$ is the exciton energy at T = 0 K, α is the temperature coefficient, and β is a parameter related to the Debye temperature of the crystal.[34] Good fits to the NW FXA data were obtained using the fitting parameters of $E(0)$ = 2.536 eV, α = 0.00039 eV/K, and β = 312 K for a CdS bulk crystal.[35] The excellent agreement between the fit and the data indicates

that the observed temperature dependence is intrinsic to the CdS NW. The trends of FXB-LO and FXB-2LO follow the exciton peak closely as temperature increases. This clearly supports that the FXB-LO and FXB-2LO are indeed excitonic in origin (as we have identified) and are not impurity-related. As the binding energy of the bound excitons in CdS is not much more than 20 meV, they will be ionized at RT (k_BT ~25 meV) and would not be observed.[36] Therefore, the BE spectrum of CdS NWs at room temperature is dominated by the radiative recombination of FXA.

Despite the extensive studies on the PL recombination dynamics of CdS nanostructures, there has been much confusion over their recombination mechanisms as various mechanisms have been ascribed to different CdS nanostructures which include NWs and nanocrystals (NCs).[10, 25-28] For example, Titova *et al.* had measured the recombination dynamics in single CdS NWs and had assigned the short lifetime (<80 ps) as being dominated by the non-radiative surface recombination; and the longer recombination lifetimes to the spatially localized states.[37] Matsuura *et al.*, on the other hand investigated the PL decay dynamics of CdS NCs embedded in Al_2O_3 matrix and attributed the short and long decay lifetimes at high temperatures to the recombination of free-excitons and shallowly-trapped excitons, respectively.[38] A surface modification study (utilizing PMMA coating of the NWs) will allow us to elucidate the appropriate origins of the lifetime components in our CdS NWs.[39] Figure 3(a) shows the TRPL spectra of the same individual CdS NW (with diameter ~120 nm) before and after coating with PMMA. The PL decay was monitored at an energy of 2.45 eV.

Prior to the PMMA-coating, the decay transients can be fitted using a bi-exponential decay function expressed as follows:

$$I(t) = A_1 \exp(-t / \tau_1) + A_2 \exp(-t / \tau_2), \quad (2)$$

where A_1 and A_2 are the amplitudes (or weighting factors); and τ_1 and τ_2 are the corresponding lifetimes. The red solid lines are the fitted curves based on equation (2), where τ_1 and τ_2 are found to be 0.15 ± 0.08 ns and 0.42 ± 0.08 ns, respectively. The short component τ_1 is ascribed to the surface related non-radiative recombination processes and the long lifetime is attributed to the recombination of free excitons in CdS NWs.[40] Our assignment is based on the following analysis: PMMA coating of the NWs is expected to suppress the contributions from the surface states, which indeed resulted in only the longer decay lifetime (0.59 ± 0.08 ns) remaining. Further validation of their origins is obtained from the integrated PL spectra of the CdS NWs with different diameters (*i.e.*, 80 nm to 315 nm). Enhanced BE emission is observed following PMMA coating (Figure 3(b) – (e)). This is attributed to the passivation of the NW surface containing a large amount of defects that contribute to the non-radiative pathways. It should be noted that a thin film of PMMA would change the dielectric environment of the CdS NWs and affect the outcoupling of the photons. The thickness of the PMMA film in our experiment is estimated to be around 200 nm. Given that the refractive index of CdS NW, PMMA and air (at 500 nm wavelength) are 2.82, 1.49 and 1.00 respectively, we can estimate the outcoupling efficiency of bare CdS NW and PMMA-CdS NW – as shown in a schematic in Figure S1 (a) and (b). For a fixed collecting lens, after coating with PMMA film the collecting efficiency is evidently decreased due to the

large refraction angle (β) compared to the incidence angle (α).The objective used in our experiment is a Nikon 50 × (N.A.= 0.55, sin α = 0.55) and the outcoupling efficiency after coating with PMMA is estimated to decrease by ~63%. Even with this decrease in coupling efficiency after PMMA coating, the increased PL signal measured from the CdS NW after PMMA coating is clear evidence that the PMMA film actually passivates the CdS NW surface, yielding enhanced emission. FTIR measurements revealed the absence of any strong chemical interactions between the PMMA and CdS (see supporting information Figure S2) even though it has a passivating effect on the CdS surface dangling bonds. The surface/interfacial effects of PMMA on the CdS NW surface are very complex topics by themselves and are certainly non-trivial.[41, 42] However, it is not the focus of this work to unravel their interaction mechanisms.

The surface related PL component (*i.e.*, PL quenched by the dark surface states) can then be estimated from the expression $(I_{\text{w/t PMMA}} - I_{\text{w/o PMMA}})/I_{\text{w/t PMMA}}$. With increasing NW diameter, the percentage of surface related PL decreases, as shown in Figure 3(f). This behaviour is consistent with the reduction of the surface-to-volume ratio for the thicker CdS NWs. With a high surface-to-volume ratio in the thinner NWs, surface defects, near surface traps and surface adsorbed species, offering alternative relaxation pathways for the de-excitation of photo-excited carriers, play a significant role in the carrier relaxation dynamics in these one dimensional systems.[43] It is extremely challenging to experimentally measure the quantum yield of a single CdS NWs. Given that our data in Fig 3(b) – (e) showed an increase in emission intensity (after PMMA coating) under the same

photo-excitation conditions (*i.e.*, the same optical setup and for the same NW), it is therefore reasonable that our PMMA-coated NWs exhibited an increase in PL quantum efficiency $\Phi = \frac{\#\ of\ photons\ emitted}{\#\ of\ photons\ absorbed}$. Further discussion on the increase in PL emission can be found in the supporting information (see Figure S1). In addition, contributions from the donor bound excitons could also be discounted as the TRPL measurements were performed at room temperature. Hence, we can attribute the fast and slow decay lifetimes to originate from the recombination of excitons near the surface and at the "bulk", respectively; or more generally from the defect-rich regions near the surface (*i.e.*, dominated by the non-radiative component) and the defect-free regions located within the NW "bulk" (*i.e.*, dominated by the radiative component).

The influence of NW diameter on the recombination rate in single CdS NWs was also investigated. Figure 4(a) shows the TRPL data from single NWs (without PMMA coating) with comparable lengths of 8 μm and with diameters ranging from 80 nm to 315 nm. The red solid lines are fitting curves based on equation (2). The decay lifetimes and their respective weighting factors (in %) are listed in Table 1. Figure 4(b) shows the decay transients from the same NWs following PMMA coating and they were fitted with a single exponential function (with decay lifetime τ'_2). Both the fast (τ_1) and slow (τ_2) decay lifetimes exhibit an increasing trend as the CdS NW diameter increases as shown in Figure 4(c) and (d). A similar trend is also obtained for τ'_2 (after PMMA coating). Although similar trends had also been previously reported for CdS NCs and ZnO NWs, the mechanisms need not be the same.[44-46] Henceforth, we shall focus on the mechanisms in our NWs. In our case, CdS NWs have diameters ranging

from 80 to 315 nm which is significantly larger than the exciton Bohr radius (~ 2.8 nm),[39] therefore there are no quantum confinement effects in these NWs. In addition, the surface depletion induced quantum confinement effect reported for CdS nanobelts could also be excluded in our NWs as the PMMA coating of the NWs would strongly weaken the surface depletion effect.[12]

Table 1 shows the relative fractional intensity ($A_i \cdot \tau_i$) of each lifetime component. The fast lifetime is dominant in the smaller NWs (*e.g.*, ~56.5 % in the 80 nm NW) and its contribution increases with decreasing NW diameter – consistent with the increasing surface-to-volume ratio in the thinner NWs. This results in a fast decay in the hundreds of picoseconds. After PMMA coating, the fast component is suppressed and the remaining lifetime τ'_2 is comparable to τ_2 (without PMMA coating). The slow decay component $\tau_{2,}$ is attributed to the FXA recombination from within the "bulk" region of NWs. The decay lifetime (~0.4-1.2 ns) is comparable to that measured for bulk CdS (~0.5-1.0 ns),[47] but is significantly longer than some reported single CdS NW studies (~80 ps) and nanosheets (~200 ps).[37, 48] This long exciton decay lifetime attests the high quality nature of our as-synthesized sample. In general, the PL decay rate is a sum of the radiative and non-radiative decay rates:

$$\tau_{PL}^{-1} = \tau_R^{-1} + \tau_{NR}^{-1}, \quad (3)$$

where τ_{PL}, τ_R and τ_{NR} are the PL, radiative and non-radiative decay time constants, respectively. The decrease in the PL decay rate with increasing NW diameters may arise from either a decrease in $1/\tau_R$ or a decrease in $1/\tau_{NR}$. Possible origins for the former includes: (1)

surface scattering effects[49] and (2) exciton-polariton effects; while those for the later includes: (3) the effects of a non-uniform defect concentration over the NW diameter, or (4) surface state effects. Amongst these possible effects, only surface scattering effect (1) is the most likely origin for the decrease in PL decay rate. In the former (radiative) case, (2) the exciton-polariton effect is dominant in the case where the NW dimension is comparable to the emission wavelength (*i.e.*, ~hundreds of nm)[50]. The CdS NWs are typically tens of micrometers long, so this effect is not likely to have a big contribution to the radiative recombination rate. Furthermore, the PL decay rates versus the CdS NW diameter do not follow a linear relationship.[50] The nonlinear behaviour between the decay rates and NW diameter also suggests that the exciton-polariton effect is not effective here. The latter (non-radiative) effects could also be discounted as: (3) all the samples were grown under the same conditions and it is reasonable that the NW "bulk" amongst the samples would have almost the same amount of defects (on average); and (4) surface states would only have a dominating effect on the surface related fast recombination lifetimes.

Lastly, we shall discuss the surface scattering effects (1). Given that the exciton diffusion length in CdS films is ~650 nm (at RT)[51, 52] and our NWs have a diameter ranging from 80 nm to 315 nm, it is plausible that the excitons would have undergone scattering or interaction with the NW surface many times before eventually decaying to the ground states. Such scattering events or interactions make them even more susceptible to trapping at the surface defect states. This effect would be more significant in the thinner NWs than the thicker ones (Figure 4(d)). However, this scattering mechanism is different from that of the

non-radiative surface trapping effect (3). This is because after PMMA coating of the NWs, τ'_2 remains relatively comparable to but still larger than the values of τ_2 (prior to the PMMA coating). This larger value (see Figure 4(d)) is consistent with the quenching of the surface trapping sites, thus permitting longer effective "scattering lengths" and hence the longer τ'_2. We are therefore convinced that this scattering mechanism (1) plays an important role in the nanostructure size dependent exciton recombination dynamics. Following this interpretation, one can expect that the two lifetimes should diverge with decreasing NW diameter. From figure 4d, we do see a diverging trend - the two lifetimes are almost overlapped when the NW diameter is large, while the two lifetimes diverge when the NW diameter is small (though it appears that the lifetime converges for the smallest size (within the reported error). We must acknowledge that although surface scattering play a dominant role here, other factors such as the non-passivated area which is in contact with the substrate and the effective thickness of the PMMA layer on top of the NW will also have some effect on the exciton lifetime. Interplay of these effects will smear out the distinct trends and this interplay is more severe in the smaller NWs. Hence, we can only expect an approximate trend for the free exciton lifetimes before and after passivation as a function of NW diameter.

CONCLUSIONS

In summary, we present a comprehensive temperature-dependent and TRPL study on the size-dependent exciton decay dynamics of high quality CdS NWs fabricated by the VLS method. Two exciton decay channels, with a short lifetime τ_1 and a long lifetime τ_2, are respectively identified as originating from (a) surface states related non-radiative

recombination and (b) free-exciton A (FXA) radiative recombination. As the NW diameter decreases from 315 nm to 80 nm, the FXA decay rate increases monotonically. TRPL measurements, together with surface passivation treatments, verified that the increasing FXA decay rate is attributed to the enhanced surface scattering in thinner NWs. The surface state related non-radiative decay rate also increases with decreasing NW diameter as a result of the larger surface-to-volume ratio in the thinner NWs. Our findings have discerned the interplay between these effects and advanced the understanding of size-dependent optoelectronic properties of 1-D semiconductor nanostructures.

ACKNOWLEDGEMENTS

T.C.S. acknowledges the support from the following research grants: NTU start-up grant (M58110068) and Ministry of Education AcRF Tier 2 Grant MOE2011-T2-2-051 (M402110000). X.L. and T.C.S. also acknowledge the financial support by the Singapore National Research Foundation (NRF) through the Competitive Research Programme (CRP) under Project No. NRF-CRP5-2009-04 and the Singapore-Berkeley Research Initiative for Sustainable Energy (SinBeRISE) CREATE Programme. Q.X. thanks the strong support from Singapore National Research Foundation through a Fellowship grant (NRF-RF2009-06) and a Competitive Research Program (NRF-CRP-6-2010-2). He also acknowledges the very strong support from Nanyang Technological University via start-up grant (M58110061) and New Initiative Fund (M58110100).

Supporting Information

A schematic of the out-coupling efficiency and FTIR spectra. This information is available free of charge via the Internet at http://pubs.acs.org.

Figure and table captions:

Figure 1. (a) X-ray diffraction pattern of the as-prepared sample. (b) PL spectrum of a typical CdS NW taken at room temperature. The insets are the TEM and HRTEM images of CdS NW grown along the [001] direction. The unlabeled scale bar is 50 nm. (c) PL spectrum of CdS nanowire taken at 77 K. Open circles are the experimental data, while the solid red line is the multi-Gaussian fit of the spectra and the deconvolved peaks are given by the blue solid lines.

Figure 2. (a) Temperature-dependent steady-state PL spectra of a CdS NW sample with a diameter of ~200 nm obtained at an excitation density of ~10 mW/cm^2. All the data were normalized by the FXA intensity and the solid lines follow the peak positions. (b) Temperature-dependent PL peak positions of FXB, FXA, FXB-LO and FXB-2LO. The solid line is the fitting curve using the Varshni equation.

Figure 3. (a) TRPL spectra at ~2.45 eV for CdS NW with a diameter of 120 nm before and after coating with PMMA. (b)-(d) PL spectra acquired from CdS NWs of different diameters – before and after coating PMMA. The inset is the corresponding SEM image. The excitation wavelength is 405 nm with an excitation density ~10 mW/cm^2. (f) Percentage of surface PL as a function of NW diameter.

Figure 4. (a) TRPL spectra at ~2.45 eV for CdS NWs with different diameters, the solid red lines are the fitting curves using a bi-exponential decay function. (b) TRPL spectra of the NW samples shown in (a) after coating with PMMA. The solid red lines are the fitting curves using a mono-exponential decay function. (c) and (d) Decay lifetimes τ_1 and τ_2 from CdS NWs with and without PMMA coating as a function of NW diameter.

Table I. Decay constants and the amplitudes obtained from the fits based on equation 2.

Figure 1

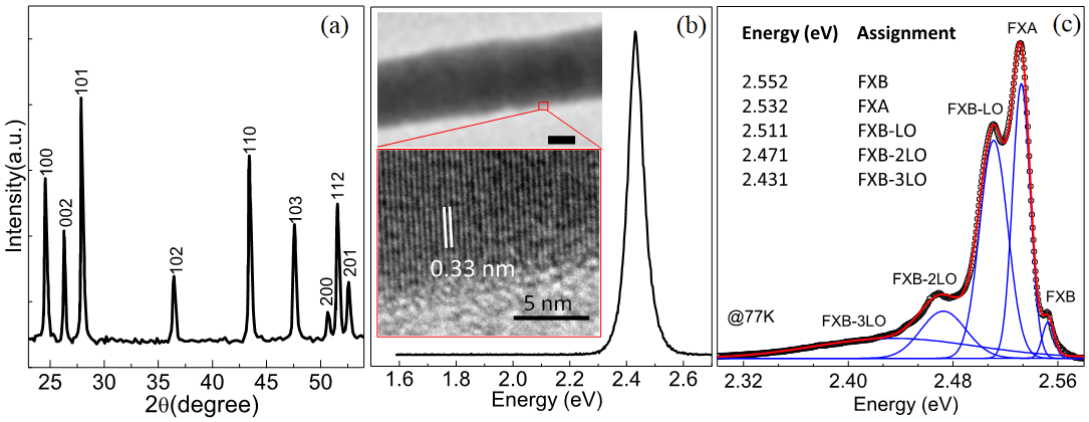
(a)
Intensity(a.u.)
100
002
101
102
110
103
200
112
201
25 30 35 40 45 50
2θ(degree)
(b)
0.33 nm
5 nm
1.6 1.8 2.0 2.2 2.4 2.6
Energy (eV)
(c)
Energy (eV) Assignment
2.552 FXB
2.532 FXA
2.511 FXB-LO
2.471 FXB-2LO
2.431 FXB-3LO
FXA
FXB-LO
FXB-2LO
FXB
FXB-3LO
@77K
2.32 2.40 2.48 2.56
Energy (eV)

Figure 2

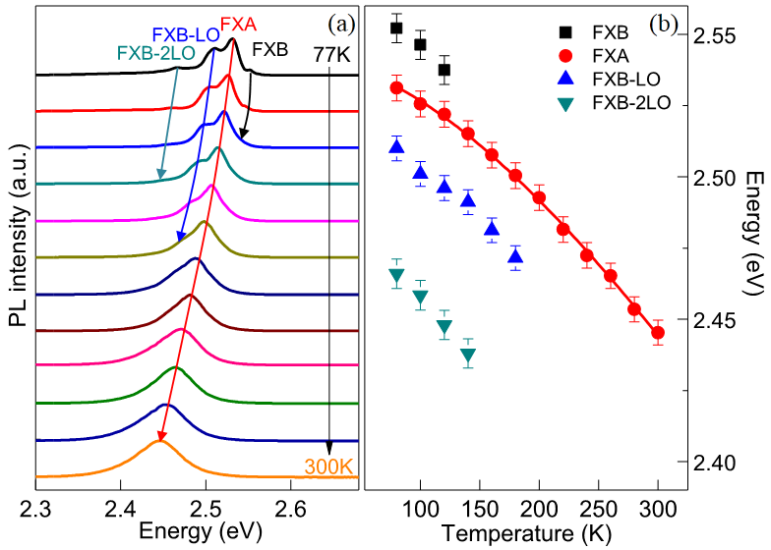
(a)
FXB-LO
FXA
FXB-2LO
FXB
77K
300K
PL intensity (a.u.)
2.3
2.4
2.5
2.6
Energy (eV)
(b)
FXB
FXA
FXB-LO
FXB-2LO
2.55
2.50
2.45
2.40
Energy (eV)
100
150
200
250
300
Temperature (K)

Figure 3

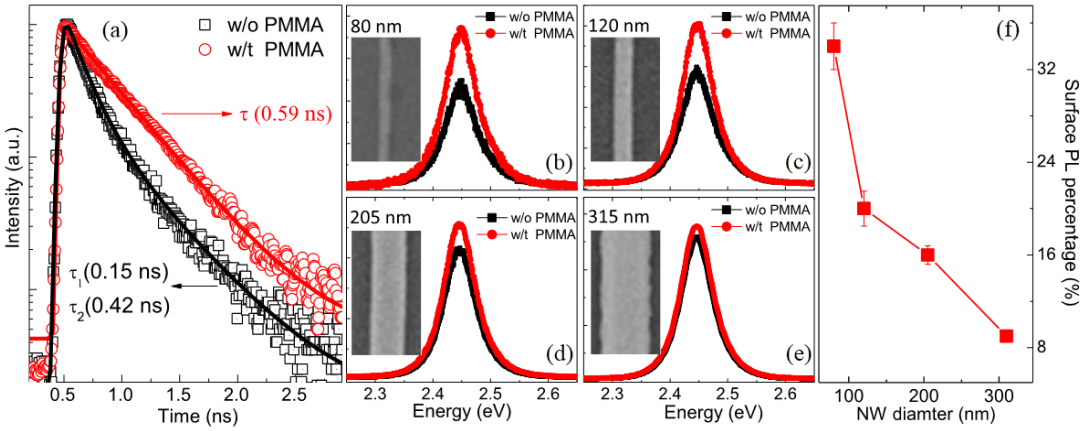
(a)
w/o PMMA
w/t PMMA
τ (0.59 ns)
τ1(0.15 ns)
τ2(0.42 ns)
Intensity (a.u.)
Time (ns)
80 nm
(b)
120 nm
(c)
205 nm
(d)
315 nm
(e)
Energy (eV)
(f)
Surface PL percentage (%)
NW diamter (nm)

Figure 4

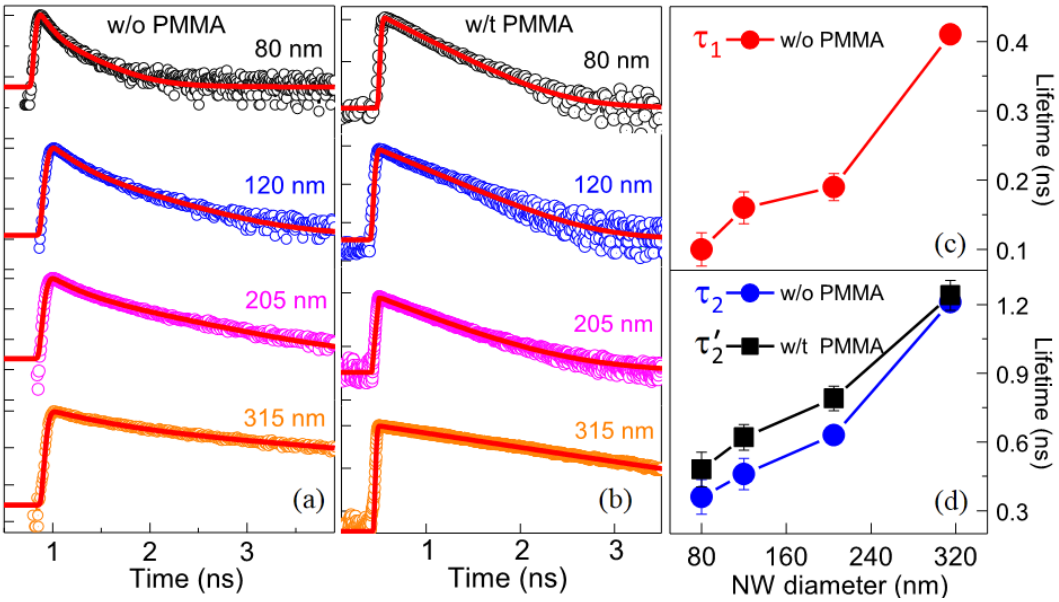
w/o PMMA
80 nm
120 nm
205 nm
315 nm
(a)
Time (ns)
w/t PMMA
80 nm
120 nm
205 nm
315 nm
(b)
Time (ns)
τ1
w/o PMMA
(c)
τ2
w/o PMMA
τ'2
w/t PMMA
(d)
Lifetime (ns)
NW diameter (nm)

Table 1

Nanowire (nm)	τ_1(ns)	τ_2(ns)	τ_2'(ns)	Weighting Factor(%) A_1	A_2
80	0.10 (±0.02)	0.36(±0.07)	0.48(±0.07)	56.5	43.5
120	0.16 (±0.02)	0.46(±0.07)	0.62(±0.07)	50.1	49.9
205	0.19 (±0.02)	0.63(±0.04)	0.79(±0.05)	40.4	59.6
315	0.42 (±0.01)	1.21(±0.03)	1.24(±0.04)	31.5	68.5

REFERENCES

(1) Lu, W.; Lieber, C. M., Semiconductor Nanowires. *Journal of Physics D-Applied Physics* **2006,** *39*, R387-R406.

(2) Reimann, S. M.; Manninen, M., Electronic Structure of Quantum Dots. *Reviews of Modern Physics* **2002,** *74*, 1283-1342.

(3) Ketterer, B.; Heiss, M.; Uccelli, E.; Arbiol, J.; Morral, A. F. I., Untangling the Electronic Band Structure of Wurtzite GaAs Nanowires by Resonant Raman Spectroscopy. *Acs Nano* **2011,** *5*, 7585-7592.

(4) Uccelli, E.; Arbiol, J.; Morante, J. R.; Morral, A. F. I., InAs Quantum Dot Arrays Decorating the Facets of GaAs Nanowires. *Acs Nano* **2010,** *4*, 5985-5993.

(5) Zhang, Q.; Zhang, J.; Utama, M. I. B.; Peng, B.; de la Mata, M.; Arbiol, J.; Xiong, Q., Exciton-phonon Coupling in Individual ZnTe Nanorods studied by Resonant Raman Spectroscopy. *Physical Review B* **2012,** *85*, 085418-085426.

(6) Liu, X. F.; Wang, R.; Jiang, Y. P.; Zhang, Q.; Shan, X. Y.; Qiu, X. H., Thermal Conductivity Measurement of Individual CdS Nanowires using Microphotoluminescence Spectroscopy. *Journal of Applied Physics* **2010,** *108*, 054310-054313.

(7) Zhang, Q.; Shan, X. Y.; Feng, X.; Wang, C. X.; Wang, Q. Q.; Jia, J. F.; Xue, Q. K., Modulating Resonance Modes and Q Value of a CdS Nanowire Cavity by Single Ag Nanoparticles. *Nano Letters* **2011,** *11*, 4270-4274.

(8) Zhang, Q.; Liu, X.; Utama, M. I. B.; Zhang, J.; de la Mata, M.; Arbiol, J.; Lu, Y.; Sum, T. C.; Xiong, Q., Highly Enhanced Exciton Recombination Rate by Strong Electron–Phonon Coupling in Single ZnTe Nanobelt. *Nano Letters* **2012,** *12*, 6420-6427.

(9) Li, Y.; Qian, F.; Xiang, J.; Lieber, C. M., Nanowire Electronic and Optoelectronic Devices. *Materials Today* **2006,** *9*, 18-27.

(10) Li, D. H.; Zhang, J.; Zhang, Q.; Xiong, Q. H., Electric-Field-Dependent Photoconductivity in CdS Nanowires and Nanobelts: Exciton Ionization, Franz Keldysh, and Stark Effects. *Nano Letters* **2012,** *12*, 2993-2999.

(11) Xu, X. L.; Zhao, Y. Y.; Sie, E. J.; Lu, Y. H.; Liu, B.; Ekahana, S. A.; Ju, X.; Jiang, Q. K.; Wang, J. B.; Sun, H. D.; Sum, T. C.; Huan, C. H. A.; Feng, Y. P.; Xiong, Q. H., Dynamics of Bound Exciton Complexes in CdS Nanobelts. *Acs Nano* **2011,** *5*, 3660-3669.

(12) Spinelli, P.; Ferry, V. E.; van de Groep, J.; van Lare, M.; Verschuuren, M. A.; Schropp, R. E. I.; Atwater, H. A.; Polman, A., Plasmonic Light Trapping in Thin-film Si Solar Cells. *Journal of Optics* **2012,** *14*.

(13) Woggon, U.; Hild, K.; Gindele, F.; Langbein, W.; Hetterich, M.; Grun, M.; Klingshirn, C., Huge Binding Energy of Localized Biexcitons in CdS/ZnS Quantum Structures. *Physical Review B* **2000,** *61*, 12632-12635.

(14) Liu, X.; Zhang, Q.; Xiong, Q.; Sum, T. C., Tailoring the Lasing Modes in Semiconductor Nanowire Cavities using Intrinsic Self-Absorption. *Nano Letters* **2013,** *13*, 1080-1085.

(15) Agarwal, R.; Barrelet, C. J.; Lieber, C. M., Lasing in Single Cadmium Sulfide Nanowire Optical Cavities. *Nano Letters* **2005,** *5*, 917-920.

(16) Liu, B.; Chen, R.; Xu, X. L.; Li, D. H.; Zhao, Y. Y.; Shen, Z. X.; Xiong, Q. H.; Sun, H. D., Exciton-Related Photoluminescence and Lasing in CdS Nanobelts. *Journal of Physical Chemistry C* **2011,** *115*, 12826-12830.

(17) Oulton, R. F.; Sorger, V. J.; Zentgraf, T.; Ma, R. M.; Gladden, C.; Dai, L.; Bartal, G.; Zhang, X., Plasmon lasers at Deep Subwavelength Scale. *Nature* **2009,** *461*, 629-632.

(18) Cho, C. H.; Aspetti, C. O.; Turk, M. E.; Kikkawa, J. M.; Nam, S. W.; Agarwal, R., Tailoring Hot-exciton Emission and Lifetimes in Semiconducting Nanowires via Whispering-gallery Nanocavity Plasmons. *Nature Materials* **2011,** *10*, 669-675.

(19) Zhang, J.; Li, D. H.; Chen, R.; Xiong, Q. H., Laser cooling of a Semiconductor by 40 Kelvin. *Nature* **2012,** *doi:10.1038/nature11721*.

(20) Kambhampati, P., Unraveling the the Structure and Dynamics of Excitons in Semiconductor Quantum Dots. *Accounts of Chemical Research* **2011,** *44*, 1-13.

(21) Block, S. B.; Yurs, L. A.; Pakoulev, A. V.; Selinsky, R. S.; Jin, S.; Wright, J. C., Multiresonant Multidimensional Spectroscopy of Surface-Trapped Excitons in PbSe Quantum Dots. *Journal of Physical Chemistry Letters* **2012,** *3*, 2707-2712.

(22) Vietmeyer, F.; Frantsuzov, P. A.; Janko, B.; Kuno, M., Carrier Recombination Dynamics in Individual CdSe Nanowires. *Physical Review B* **2011,** *83*, 115319.

(23) Lo, S. S.; Major, T. A.; Petchsang, N.; Huang, L.; Kuno, M. K.; Hartland, G. V., Charge Carrier Trapping and Acoustic Phonon Modes in Single CdTe Nanowires. *ACS Nano* **2012,** *6*, 5274-5282.

(24) van Vugt, L. K.; Piccione, B.; Cho, C. H.; Aspetti, C.; Wirshba, A. D.; Agarwal, R., Variable Temperature Spectroscopy of As-Grown and Passivated CdS Nanowire Optical Waveguide Cavities. *Journal of Physical Chemistry A* **2011,** *115*, 3827-3833.

(25) van Vugt, L. K.; Veen, S. J.; Bakkers, E.; Roest, A. L.; Vanmaekelbergh, D., Increase of the Photoluminescence Intensity of InP Nanowires by Photoassisted Surface Passivation. *Journal of the American Chemical Society* **2005,** *127*, 12357-12362.

(26) Park, W. I.; Kim, J. S.; Yi, G. C.; Bae, M. H.; Lee, H. J., Fabrication and Electrical Characteristics of High-performance ZnO Nanorod Field-effect Transistors. *Applied Physics Letters* **2004,** *85*, 5052-5054.

(27) Cha, S. N.; Jang, J. E.; Choi, Y.; Ho, G. W.; Kang, D. J.; Hasko, D. G.; Welland, M. E.; Amaratunga, G. A. J., High performance ZnO nanowire Field-effect Transistor. In *Proceedings of Essderc 2005: 35th European Solid-State Device Research Conference*, Ghibaudo, G.; Skotnicki, T.; Cristoloveanu, S.; Brillouet, M., Eds. 2005; pp 217-220.

(28) Barrelet, C. J.; Wu, Y.; Bell, D. C.; Lieber, C. M., Synthesis of CdS and ZnS Nanowires using Single-source Molecular Precursors. *Journal of the American Chemical Society* **2003,** *125*, 11498-11499.

(29) Cao, B. L.; Jiang, Y.; Wang, C.; Wang, W. H.; Wang, L. Z.; Niu, M.; Zhang, W. J.; Li, Y. Q.; Lee, S. T., Synthesis and Lasing Properties of Highly Ordered CdS Nanowire Arrays. *Advanced Functional Materials* **2007,** *17*, 1501-1506.

(30) Langer, D. W.; Euwema, R. N.; Era, K.; Koda, T., Spin Exchange in Excitons, the Quasicubic Model and Deformation Potentials in II-VI Compounds. *Physical Review B-Solid State* **1970,** *2*, 4005-4022.

(31) Lovergine, N.; Cingolani, R.; Mancini, A. M.; Ferrara, M., Photoluminescence of CVD Grown CdS Epilayers on CdTe Substrates. *Journal of Crystal Growth* **1992,** *118*, 304-308.

(32) à la Guillaume, C. B.; Debever, J.-M.; Salvan, F., Radiative Recombination in Highly Excited CdS. *Physical Review* **1969,** *177*, 567-580.

(33) Thomas, D. G.; Hopfield, J. J., Optical Properties of Bound Exciton Complexes in Cadmium Sulfide. *Physical Review* **1962,** *128*, 2135-&.

(34) Vurgaftman, I.; Meyer, J. R.; Ram-Mohan, L. R., Band Parameters for III-V Compound Semiconductors and their Alloys. *Journal of Applied Physics* **2001,** *89*, 5815-5875.

(35) Imada, A.; Ozaki, S.; Adachi, S., Photoreflectance Spectroscopy of Wurtzite CdS. *Journal of Applied Physics* **2002,** *92*, 1793-1798.

(36) Zhang, J. M.; Ruf, T.; Lauck, R.; Cardona, M., Isotope Effects on Exciton Energies in CdS. *Physical Review B* **1998,** *57*, 9716-9722.

(37) Titova, L. V.; Hoang, T. B.; Jackson, H. E.; Smith, L. M., Low-temperature Photoluminescence Imaging and Time-resolved Spectroscopy of Single CdS Nanowires. *Applied Physics Letters* **2006,** *89*, 053119-053111.

(38) Matsuura, D.; Kanemitsu, Y.; Kushida, T.; White, C. W.; Budai, J. D.; Meldrum, A., Photoluminescence Dynamics of CdS Nanocrystals Fabricated by Sequential Ion Implantation. *Japanese Journal of Applied Physics Part 1-Regular Papers Short Notes & Review Papers* **2001,** *40*, 2092-2094.

(39) Ramaiah, K. S.; Bhatnagar, A. K.; Pilkington, R. D.; Hill, A. E.; Tomlinson, R. D., The Effect of Sulfur Concentration on the Properties of Chemical Bath deposited CdS Thin Films. *Journal of Materials Science-Materials in Electronics* **2000,** *11*, 269-277.

(40) Matsuura, D.; Kanemitsu, Y.; Kushida, T.; White, C. W.; Budai, J. D.; Meldrum, A., Optical Characterization of CdS Nanocrystals in Al2O3 Matrices fabricated by Ion-beam Synthesis. *Applied Physics Letters* **2000,** *77*, 2289-2291.

(41) Cahen, D.; Hodes, G., Molecules and Electronic Materials. *Advanced Materials* **2002,** *14*, 789-798.

(42) Cohen, R.; Kronik, L.; Shanzer, A.; Cahen, D.; Liu, A.; Rosenwaks, Y.; Lorenz, J. K.; Ellis, A. B., Molecular Control over Semiconductor Surface Electronic Properties: Dicarboxylic Acids on CdTe, CdSe, GaAs, and InP. *Journal of the American Chemical Society* **1999,** *121*, 10545-10553.

(43) Li, M. J.; Xing, G. C.; Qune, L.; Xing, G. Z.; Wu, T.; Huan, C. H. A.; Zhang, X. H.; Sum, T. C., Tailoring the Charge Carrier Dynamics in ZnO Nanowires: the Role of Surface Hole/Electron Traps. *Physical Chemistry Chemical Physics* **2012,** *14*, 3075-3082.

(44) Sobhana, S. S. L.; Devi, M. V.; Sastry, T. P.; Mandal, A. B., CdS Quantum Dots for Measurement of the Size-dependent Optical Properties of Thiol-capping. *Journal of Nanoparticle Research* **2011,** *13*, 1747-1757.

(45) Reparaz, J. S.; Guell, F.; Wagner, M. R.; Hoffmann, A.; Cornet, A.; Morante, J. R., Size-dependent Recombination Dynamics in ZnO Nanowires. *Applied Physics Letters* **2010,** *96*, 53105-53107.

(46) Zhao, Q. X.; Yang, L. L.; Willander, M.; Sernelius, B. E.; Holtz, P. O., Surface Recombination in ZnO Nanorods grown by Chemical bath deposition. *Journal of Applied Physics* **2008,** *104*, 073526-073528.

(47) Heitz, R.; Hoffmann, A.; Broser, I., Exciton Dynamics in Ni-activated CdS. *Physical Review B* **1994,** *49*, 14307-14314.

(48) Rho, H.; Lee, K. Y.; Hoang, T. B.; Titova, L. V.; Mishra, A.; Smith, L. M.; Jackson, H. E.; Yarrison-Rice, J. M.; Choi, Y. J.; Choi, K. J.; Park, J. G., Spatially-resolved Photoluminescence Mapping of Single CdS Nanosheets. *Applied Physics Letters* **2008,** *92*, 013111-013113.

(49) Gil, B.; Kavokin, A. V., Giant Exciton-light Coupling in ZnO Quantum Dots. *Applied Physics Letters* **2002,** *81*, 748-750.

(50) Hong, S. S.; Joo, T.; Park, W. I.; Jun, Y. H.; Yi, G. C., Time-resolved Photoluminescence of the Size-controlled ZnO Nanorods. *Applied Physics Letters* **2003,** *83*, 4157-4159.

(51) Weber, C.; Becker, U.; Renner, R.; Klingshirn, C., Measurement of the Diffusion-length of Carriers and Excitons in CdS using Laser-induced Transient Gratings. *Zeitschrift Fur Physik B-Condensed Matter* **1988,** *72*, 379-384.

(52) Kippelen, B.; Grun, J. B.; Honerlage, B.; Levy, R., Transient Optical Nonlinearities in CdS studied by Laser-induced Grating Spectroscopy at Room-temperature. *Journal of the Optical Society of America B-Optical Physics* **1991,** *8*, 2363-2369.

TOC graphic

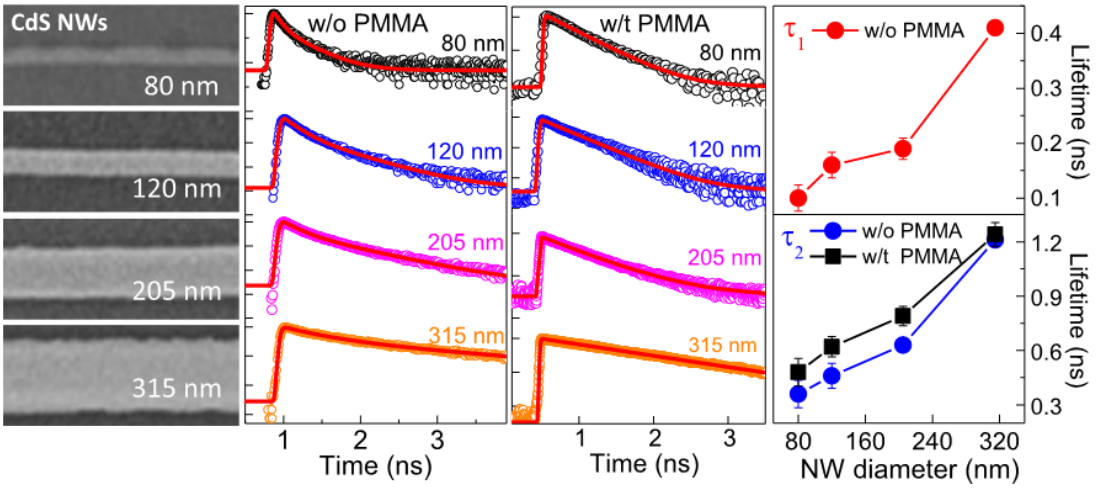
CdS NWs
80 nm
120 nm
205 nm
315 nm
w/o PMMA
w/t PMMA
Time (ns)
Time (ns)
τ1
τ2
w/o PMMA
w/t PMMA
Lifetime (ns)
Lifetime (ns)
NW diameter (nm)